IEEE Access
Multidisciplinary | Rapid Review | Open Access Journal

Date of publication xxxx 00, 0000, date of current version xxxx 00, 0000.

Digital Object Identifier 10.1109/ACCESS.2017.DOI

An Adaptive Region Growing based on Neutrosophic Set in Ultrasound Domain for Image Segmentation

XUE JIANG[1,2], YANHUI GUO[3], HAIBIN CHEN[1], YAQIN ZHANG [4] AND YAO LU[1,2,5].

[1]School of Data & Computer Science, Sun Yat-sen University, Guangzhou, China
[2]Guangdong Province Key Laboratory of Computational Science, Sun Yat-sen University, Guangzhou, China
[3]Department of Computer Science, University of Illinois Springfield, Springfield, IL, USA
[4]Department of Radiology, The fifth Affiliated Hospital of Sun Yat-sen University
[5]Department of Ultrasound, The fifth Affiliated Hospital of Sun Yat-sen University

Corresponding author: Yao Lu (e-mail: luyao23@mail.sysu.edu.cn) and Yaqin Zhang (e-mail: zhyaqin@mail.sysu.edu.cn).

This study was supported by grants from the China Department of Science and Technology Key Grant (No. 2018YFC1704206, 2016YFB0200602), NSFC (No. 81801809,81830052, 11401601), the Science and Technology Innovative Project of Guangdong Province(No. 2016B030307003, 2015B010110003, and 2015B020233008), Guangdong Provincial Science and Technology Key Grant (No. 2017B020210001), Guangzhou Science and Technology Creative Key Grant (No. 201604020003), and Guangdong Province Key Laboratory of Computational Science Open Grant(No. 2018009).

ABSTRACT Breast tumor segmentation in ultrasound is important for breast ultrasound (BUS) quantitative analysis and clinical diagnosis. Even this topic has been studied for a long time, it is still a challenging task to segment tumor in BUS accurately arising from difficulties of speckle noise and tissue background inconsistence. To overcome these difficulties, we formulate breast tumor segmentation as a classification problem in the neutrosophic set (NS) domain which has been previously studied for removing speckle noise and enhancing contrast in BUS images. The similarity set score and homogeneity value for each pixel have been calculated in the NS domain to characterize each pixel of BUS image. Based on that, the seed regions are selected by an adaptive Otsu-based thresholding method and morphology operations, then an adaptive region growing approach is developed for obtaining candidate tumor regions in NS domain. The direction of region growing depends on the differences of similarity set score, texture homogeneity value and distance value between the seed region and the candidate growing points. A deep convolutional neural network, based on VGG-16 network, is applied to each candidate tumor region for false positive reduction. A testing dataset with pathology proof includes 35 images without tumor, 36 images with benign tumors and 50 images with malignant tumors. Numerical experiments show that the proposed method is effective to segment breast tumor in BUS images with average 81.6% and 84.4% percent dice coefficient, average 77.0% and 84.3% true positive ratio, average 11.2% and 15.2% false positive ratio, and average 57.5 $pixel$ and 52.8 $pixel$ Hausdorff distance for benign and malignant images, respectively.

INDEX TERMS Breast ultrasound; Image segmentation; Neutrosophic set; Region growing; Similarity set score.

I. INTRODUCTION

BREAST cancer is one of the leading causes among women worldwide [1]. Early detection of breast cancer is important in clinic to improve patient survival [2]. Breast Ultrasound (BUS) is a cost efficient and noninvasive imaging tool for early detection of breast cancer [3]. Quantitative analysis of breast cancer including accurate measurement of tumor region of interest (ROI), is an essential step in clinical diagnosis. Currently in clinical setting, doctors visually segment tumor ROI and measure parameters by hand which is relatively subjective and depends on the doctor experience. To overcome this difficulty, computer-aided detection (CAD) system [4] intends to exploit machine learning technology to automatically segment tumor ROI for future clinical measurement or quantitative analysis. Breast cancer segmentation in BUS has been studied in different context by previous researchers, however, it still needs improvement of segmentation accuracy for clinical applications with difficul-

This article has been accepted for publication in a future issue of this journal, but has not been fully edited. Content may change prior to final publication. Citation information: DOI 10.1109/ACCESS.2019.2911560, IEEE Access

ties of speckle noise and tissue background inconsistence.

Most existing segmentation methods for BUS has been borrowed from general image processing field. These segmentation methods in the literature fall into four classes: gray-level thresholding method, active contour method, graph-based approaches and learning-based approaches [1]. These methods based on different hypothesis have different advantages and disadvantages, and it is difficult to overcome the segmentation difficulty in BUS by a single method. To optimize the segmentation results, hybrid techniques have been widely used in previous studies.

Gray-level thresholding is fast and straightforward for tumor segmentation in BUS using the gray value difference between tumor and tissue background, which has been widely used as pre-processing technique for other segmentation methods [5]. Selecting an appropriate threshold value is crucial for differentiating tumor pixels from background pixels. A single global thresholding value is simple however inefficient for segmentation purpose, which is usually used to generate seed points for other approaches. In most fast segmentation applications, locally adaptive thresholding value depending on local texture features and gray value pattern has been efficiently used for fast tumor segmentation in BUS.

The active contour method has been widely used for tumor segmentation especially for noisy BUS images. Most feasible semi-automated active contour methods have been proposed in previous papers, which are not practical in a clinical setting since the users are required to outline the initial contour for further segmentation. An automated active contour method [6] for tumor segmentation in BUS images without human intervention has been proposed with two steps: ROI generation and ROI segmentation. A pre-trained texture classifier using the tissue background pattern has been trained to select the ROI candidates, and then an active contour model, combining both global gray-level statistical information and local edge information, is applied for approximate the tumor contour. [7] defines a global active contour model and a local active contour model using the intensity statistical features of internal and external contours, and a cost functional combining both global and local region information has been minimized to automated segment tumor region in BUS images.

Graph-based approaches are used in BUS image segmentation after the success in general image segmentation. In a graph model, the BUS image is initialized with a segmentation label, and then the probability of which label each pixel belonging to is calculated for classification. [8] combines maximum a posteriori (MAP) and Markov random field (MRF) to estimate the BUS images distortion field with labeling image regions based on the corrected intensity statistics. This method contains two steps, the MAP step estimates the intensity model parameters and the MRF step describes the distributions of image tissue classes.

Image segmentation can be modelled as a learning-based classification problem which classifies the pixels into background pixels and foreground pixels. Learning-based methods are categorized into two groups: unsupervised and supervised method. Fuzzy C-means (FCM) is an effective unsupervised learning approach for breast cancer segmentation in BUS images. In the paper [9], the fuzzy c-mean clustering method is applied to detect the candidate tumors by extracting the intensity, morphology, location, and size features in the transverse, and then a logistic linear regression model is used to estimate the likelihood of these candidate regions based on the extracted features. Early in many unsupervised methods, support vector machine (SVM) [10], [11] and artificial neural network (ANN) [12], [13] are most widely used for BUS image segmentation. With the development of artificial intelligence, new deep learning techniques such as deep convolution neural networks (CNNs) and recurrent neural network (RNN) have made great progress in segmenting BUS images. In the paper [14], a novel deep learning approach, combining three different methods: a patch-based LeNet, a UNet and a pre-trained FCN-AlexNet with transfer learning, has been proposed for lesion detection in BUS images. In addition, the deep convolutional neural network can also be used for false positive reduction [15].

Some other approaches have appeared for BUS image segmentation. The paper [16] observed that a BUS image can be modelled as three regions: the lesion region, the normal tissue region, and the blurry region. Based on this observation, a fuzzy cellular automate (FAC) framework is proposed for handling the uncertain pixel during the segmentation process. Each candidate regions generated from an initial segmentation are transformed into the fuzzy domain and a voting strategy is applied to select the blurry region. The developed energy function is used to specifically classify the uncertain pixels in the blurry region. However, due to the speckle noise and low contrast of the ultrasound image, previous image processing methods have not worked satisfied in the BUS images with blurry boundary and low contrast. In addition, for less proper acquisition, some breast tumors are close to the image border and the tumor regions are cut partially which may cause failure of tumor segmentation.

To overcome the difficulties, we formulate breast tumor segmentation as a classification problem in the neutrosophic set (NS) domain which has been previously studied for removing speckle noise and enhancing contrast for segmentation in BUS images [17]. Considering of the image patterns and vagueness, a breast tumor segmentation method based on neutrosophic similarity score and region growing (NSSRG) is proposed, which achieves breast tumor segmentation by transforming the BUS images into neutrosophic set (NS) domain which consists three membership subsets with different degree of vagueness. The similarity set score and homogeneity value for each pixel have been calculated in the NS domain to characterize each pixel of BUS image for further segmentation in the NS domain. An adaptive Otsu-based thresholding method and morphology methods are used to locate seed regions, and an adaptive region growing method based on the similarity set score and homogeneity value is developed for each seed region to grow separately. A deep convolutional neural network, based on VGG-16 network,

This article has been accepted for publication in a future issue of this journal, but has not been fully edited. Content may change prior to final publication. Citation information: DOI 10.1109/ACCESS.2019.2911560, IEEE Access

is used for false positive reduction. Percent dice coefficient, true positive ratio, false positive ratio and Hausdorff Distance have been measured on various BUS images to evaluate the experiment performance.

The remaining sections are organized as follows. Section II describes the technical details of the proposed algorithm. Sections III shows the experiment results in comparing to other existing methods and an extensive discussion sequentially. Section IV concludes the present study and indicates the future research.

II. METHOD AND MATERIALS

A. METHOD

An adaptive region growing on neutrosophic set for Ultrasound image is developed for breast tumor segmentation, which includes the following four steps.

1) Domain transformation: the whole input ultrasound image is transferred into the neutrosophic set (NS) domain with speckle noise reduction and contrast enhancement;
2) Seed regions initialization: the initial seed regions are localized based on an adaptive Otsu-based thresholding method and morphology operations;
3) Region growing: according to the corresponding similarity set score vector, homogeneity vector and distance vector of candidate pixels, each seed region grows separately and finally obtaining the candidate tumor regions;
4) False positive reduction: false positive regions are reduced by a deep convolutional neural network which is based on VGG-16 network.

1) Domain transformation

Neutrosophy has been successfully used for removing speckle noise and enhancing contrast in BUS images. In NS domain, a similarity set score S is calculated to represent the probabilities of belonging to truth (T), indeterminacy (I), and falsity (F), respectively [17]. Specifically, a pixel P in BUS image I is mapped to NS domain: $P_{NS}(x,y) = \{T(x,y), I(x,y), F(x,y)\}$, where $T(x,y)$, $I(x,y)$ and $F(x,y)$ represent the elements belonging to the brightest pixel set, indeterminate pixel set, and non-white pixel set, respectively. The $T(x,y)$, $I(x,y)$ and $F(x,y)$ are calculated as follows,

$$T(x,y) = \frac{P(x,y) - P_{min}(x,y)}{P_{max}(x,y) - P_{min}(x,y)} \tag{1}$$

$$I(x,y) = \frac{Pd(x,y) - Pd_{min}(x,y)}{Pd_{max}(x,y) - Pd_{min}(x,y)} \tag{2}$$

$$F(x,y) = 1 - T(x,y) \tag{3}$$

where $P(x,y)$ and $Pd(x,y)$ are the intensity value and gradient value of pixel P in the image. $P_{min}(x,y)$ and $Pd_{min}(x,y)$ are the minimum intensity value and gradient value in the image. $P_{max}(x,y)$ and $Pd_{max}(x,y)$ are the maximum intensity value and gradient value in the image.

Here, $T(x,y)$, $I(x,y)$ and $F(x,y)$ are calculated under three image contexts: the original image I, the image M after mean filtering and the image H after texture energy measurement (TEM) filtering [18], and termed as $T_I(x,y), I_I(x,y), F_I(x,y)$, $T_M(x,y), I_M(x,y), F_M(x,y)$, and $T_H(x,y), I_H(x,y), F_H(x,y)$, respectively.

Then, under the original image context, the similarity set score $S_I(x,y)$ of the pixel P is calculated as follow,

$$S_I(x,y) = \frac{T_I(x,y)*V(1) + I_I(x,y)*V(2) + F_I(x,y)*V(3)}{\sqrt{T_I(x,y)^2 + I_I(x,y)^2 + F_I(x,y)^2} * \|V\|} \tag{4}$$

where V represents the weight vector of $T_I(x,y)$, $I_I(x,y)$ and $F_I(x,y)$. $\|V\|$ represents the model of the vector.

Under other two contexts: the image M and the image H, the simlarity set score $S_M(x,y)$ and $S_H(x,y)$ of the pixel P are calculated as described above with replacing $T_I(x,y), I_I(x,y), F_I(x,y)$ into $T_M(x,y), I_M(x,y), F_M(x,y)$ and $T_H(x,y), I_H(x,y), F_H(x,y)$, respectively.

Thus, the BUS image is transferred into NS domain by calculating the average similarity set score $S(x,y)$ of $S_M(x,y), S_I(x,y)$ and $S_H(x,y)$ for each pixel. Furthermore, the BUS images are normalizated by NS domain transformation.

2) Seed regions initialization

After transferring the BUS images into NS domain, the traditional Otsu method is applied on the transferred NS image to gain the initial threshold value of T_1. Then, the background C_0 and the foreground C_1 segmented with initial threshold value T_1 are $\{S(x,y) \geq T_1\}$ and $\{S(x,y) < T_1\}$, respectively. Since the similarity set scores of the tumor regions are commonly lower than the T_1, a new grayscale threshold T_2 is obtained by applying the traditional Otsu method on the foreground C_1 of NS image. The threshold T_2 is used to exclude background pixels with $\{S(x,y) \geq T_2\}$. The regions extracted by the above Otsu-based thresholding method are regarded as the candidate seed regions.

Then, morphology operations are performed on the foreground and background masks, individually. To fill the holes inside the seed regions, a flood-fill operation is employed on the foreground mask. The seed regions connected with the image border are deleted. To exclude small isolated background regions, disk erosion operation with radius of seven pixels and disk dilatation operation with radius of three pixels radius are sequentially performed on the background mask.

3) Region growing

In image segmentation, the goal of region growing is to divide the image domain R into background region R_b and foreground region R_f [19]–[21], which satisfy the following equations.

$$R = R_b \cup R_f \tag{5}$$

and

$$R_b \cap R_f = \emptyset \tag{6}$$

This article has been accepted for publication in a future issue of this journal, but has not been fully edited. Content may change prior to final publication. Citation information: DOI 10.1109/ACCESS.2019.2911560, IEEE Access

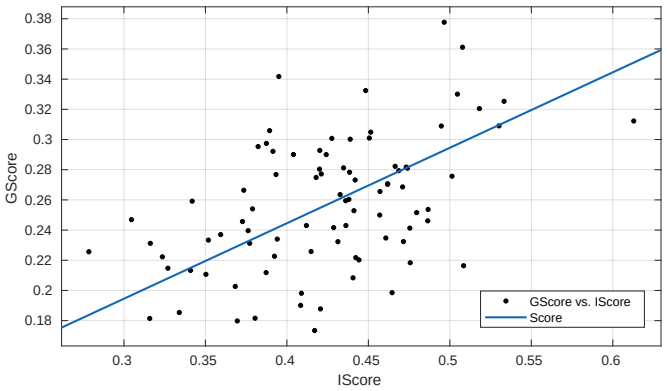

(a) relationship between $IScore$ and $GScore$

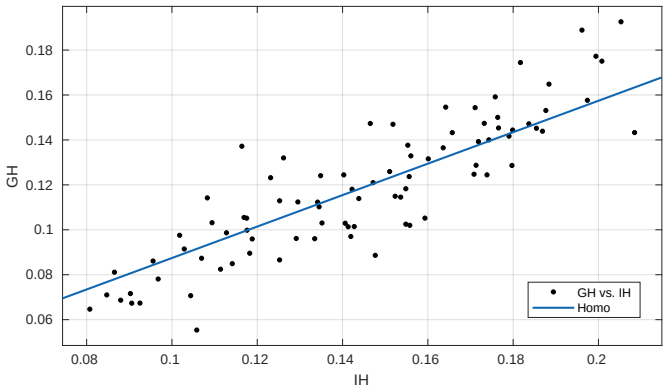

(b) relationship between IH and GH

FIGURE 1: Results of linear regression

Region growing starts with some initial seed regions $\{A_1, A_2, ..., A_n\}$. Then a seed region A_i includes m pixels $\{p_1(x_1, y_1), p_2(x_2, y_2), ..., p_m(x_m, y_m)\}$, the candidate pixels set $Clist\,\{c_1(cx_1, cy_1), c_2(cx_2, cy_2), ..., cn(cx_n, cy_n)\}$ of seed region A_i is defined as follow,

$$Clist = \bigcup_{i=1}^{m}([x_i, y_i] + Ne) \tag{7}$$

where $[x_i, y_i]$ is the position of pixel p_i in A_i. Ne is a vector which is used for obtaining the neighborhood of the pixel p_i and set as $\{-1, 0; 1, 0; 0, -1; 0, 1\}$. The pixels in A_i are not included in the $Clist$.

The direction of region growing is determined by three vectors $\{V_g, V_h, V_d\}$, which are defined as follows,

$$V_g = \bigcup_{j=1}^{n} \frac{\sum_{i=1}^{m} S(p_i)}{m} - S(c_j) \tag{8}$$

where $S(p_i)$ is the similarity set score of the pixel p_i in the seed region A_i, $S(c_j)$ is the similarity set score of the pixel c_j in the $Clist$.

$$V_h = \bigcup_{j=1}^{n} \frac{\sum_{i=1}^{m} H(p_i)}{m} - H(c_j) \tag{9}$$

where $H(p_i)$, $H(c_j)$ are the intensity values of the pixel p_i and c_i in the image H.

$$V_d = \bigcup_{j=1}^{n}(\sqrt{(cx_j - \frac{\sum_{i=1}^{m} x_i}{m})^2 + (cy_j - \frac{\sum_{i=1}^{m} y_i}{m})^2} + C) \tag{10}$$

where $[cx_i, cy_i]$ is the position of the pixel c_i in the $Clist$. C is the constant term for avoiding value zero.

For each iteration, the growth direction of each candidate seed region is defined as follow,

$$Dire = Ve(1) * V_g + Ve(2) * V_h + Ve(3) * V_d \tag{11}$$

where V_g stands for the similarity set score vector, V_h stands for the homogeneity value vector, V_d stands for the distance vector. Ve is the weight factor and set as $\{0.4, 0.4, 0.2\}$ in this study.

The pixel with the minimum value of $Dire$ among the $Clist$ is selected as the growing pixel, and would be included in set A_i. After each iteration, the pixels in $Clist$ will be updated based on the new seed regions. The stop criterion for region growing is based on the similarity set score of the image I and the intensity value of the image H. To determine the stop criterion, linear regressions are applied between the similarity set scores of the whole image I (termed as $IScore$) and the segmentation ground truth in the image I (termed as $GScore$), and between the intensity value of the whole image H (termed as IH) and the ground truth in image H (termed as GH). The results of the linear regressions are illustrated in Fig. 1.

According to the results of linear regressions, two stop criterions are set: (1) $Score_{mean}(S) \geq 0.5Score_{mean}(I)$, where $Score_{mean}(S)$ and $Score_{mean}(I)$ represent the mean similarity set scores of the seed region and the whole image I, respectively;(2) $Intensity_{mean}(S) \geq 0.7Intensity_{mean}(H)$, where $Intensity_{mean}(S)$ and $Intensity_{mean}(H)$ represent the mean intensity value of the seed region and the whole image H, respectively. The region growing stops until it meets any of the two criterion.

4) False positive reduction

The features extracted by deep convolutional neural network (DCNN) have been proved effective in reducing false positive regions [22]. In this study, a deep convolutional neural network, based on VGG-16 net, is applied for reducing the false positive regions (over segmentation). As shown in Fig. 2, a DCNN based VGG-16 network is constructed. To fit our task, the last nine layers of original VGG-16 network are replaced as new block (block 3), which is consist of dropout layer, fully connected layer and SoftMax layer. The dropout layer makes the model more generalize and prevents over-fitting [23]. The other layers of VGG-16 are kept in DCNN, as shown in blocks 1-2. Block 1 contains one max-pooling layer and two convolution layers which convolve the input images with a set of filters. Block 2 contains three convolution layers and one max-pooling layer, which can provide strong robustness and decrease the dimensions of features map. Each

This article has been accepted for publication in a future issue of this journal, but has not been fully edited. Content may change prior to final publication. Citation information: DOI 10.1109/ACCESS.2019.2911560, IEEE Access

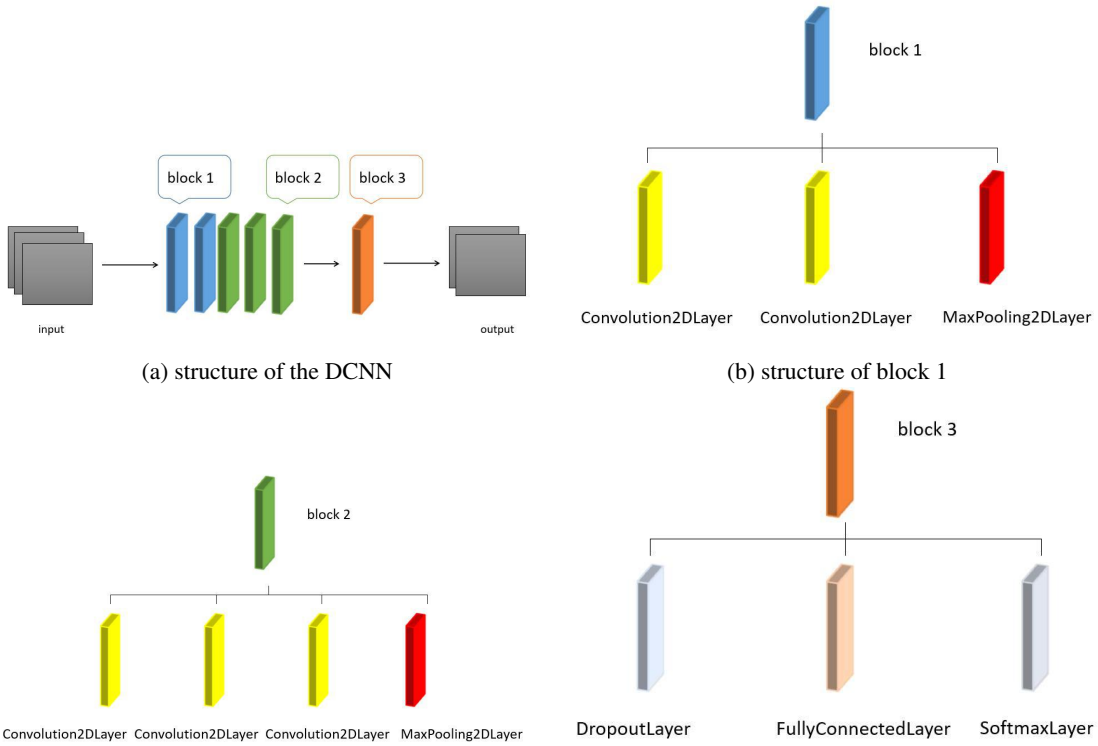

(a) structure of the DCNN

(b) structure of block 1

(c) structure of block 2

(d) structure of block 3

FIGURE 2: The structure of the proposed deep convolutional neural network (DCNN)

convolution layer in DCNN is followed by a rectified linear units (Relu) layer, which actives the feature maps extracted by the previous convolution layer with the ReLu function ($f(x) = \max(0, x)$) to improve the computation efficiency and solve the problem of disappearing gradient [24], [25].

The input images for DCNN are the candidate region images extracted from BUS image, which are generated by the following procedures: 1) cropping the maximum external quadrangle regions of candidate regions from BUS image, individually; 2) padding the quadrangle images as square images with zero; 3) resizeing the square images as size of 224×224. With the DCNN fine-tuned by BUS candidate region images, the false positive regions are removed from the candidate regions, and the breast tumor segmentation result is obtained.

With above four procedures, Fig. 3 shows the whole steps of the proposed method with a flowchart and corresponding visualization results of breast tumor segmentation using NSSRG method.

B. MATERIALS

1) Dataset

A dataset of clinical 384 BUS images, collected by VIVID 7 (GE, Horten, Norway) with 4-5 MHz linear probe, are employed in this study. The tumor contours of those images are manually delineated by experienced radiologists, which are regarded as the ground truth segmentation. 298 images of them are randomly selected for the DCNN training and the rest 86 images are used for the performance evaluation of the proposed NSSRG segmentation method. Among the 86 testing images, 36 images are benign and others are malignant, which are verified by surgeries or pathologies.

2) Quantitative criterions

To evaluate the segmentation result quantitatively, four evaluation metrics including percent dice coefficient (PDC), the false positive ratio (FPR), the true positive ratio (TPR) and Hausdorff distance (HD) are employed.

PDC is the percent of dice similar coefficient, measures the degree of overlap between segmentation results and ground truth. $PDC = 100\%$ means the segmentation results are completely consistent with the ground truth. The PDC is defined as follow,

$$PDC = \frac{2 * (A_m \cap A_g)}{A_m \cup A_g} \tag{12}$$

where A_m is the mask of segmentation result and A_g is ground truth mask. $\cap$ and $\cup$ are the intersection and union operation.

FPR represents the proportion of background pixels which are segmented as foreground. $FPR = 0$ means the segmentation results are completely correct. The FPR is defined as follow,

$$FPR = \frac{A_m / A_g}{A_g} \tag{13}$$

This article has been accepted for publication in a future issue of this journal, but has not been fully edited. Content may change prior to final publication. Citation information: DOI 10.1109/ACCESS.2019.2911560, IEEE Access

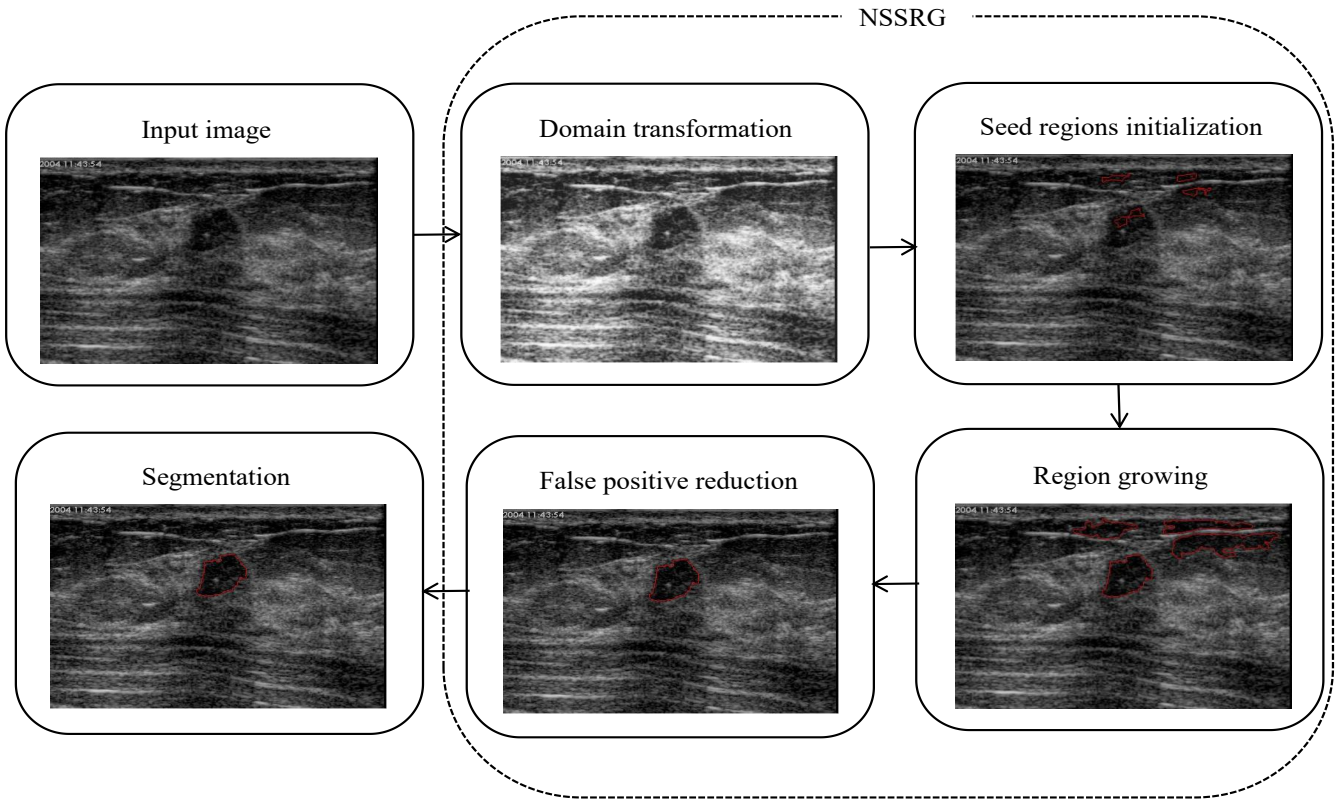

FIGURE 3: The flowchart of the proposed method

.

TPR denotes the proportion of foreground pixels which are segmented correctly. TPR ranges from zero to one and represents the worst to best segmentations, respectively. The TPR is calculated as Equation 14.

$$TPR = \frac{A_m \cap A_g}{A_g} \tag{14}$$

HD measures the differences between two contours, which is given as the maximum of the Euclidean distance between the contours of segmentation results and ground truth. Let $M\{m_1, m_2, ..., m_p\}$ and $G\{g_1, g_2, ..., g_q\}$ be the contour points of method segmented tumor and ground truth, respectively, where p and q are the quantities of contour points, the HD can be calculated as follow,

$$HD = \max\{D(M,G), D(G,M)\} \tag{15}$$

where $D(M,G) = \max_{m_i \in M}\{\min_{g_j \in G}\{Dist(m_i, g_j)\}\}$, $Dist(m_i, g_j)$ stands for the Euclidean distance between the contour point m_i in M and the contour point g_j in G. The unit of HD is $pixel$.

In this study, the proposed NSSRG segmentation method is compared with a newly published method based on the neutrosophic set score and level set (NSSLS) [17].

III. EXPERIMENTAL RESULTS

Fig. 4 illustrates the segmentation comparison between NSSLS and NSSRG on three BUS images (one of them is benign image and the others are malignant images), which have relatively clear boundary between the tumor and background. Need to be noted is that these two images in Fig.4 and the example image in Fig. 3 were also presented in Fig. 3-4 and Fig. 6 in the study of NSSLS[17]. It is observed that the NSSRG has very similar performances as the NSSLS. However, as illustrated in Fig. 5, the NSSRG achieves much superior segmentation performacnes than NSSLS on the other six BUS images (two of them are benign images and the others are malignant images). All these six images have the same characteristic: the tumor boundary is close to the image border or the shadow. In this scenario, the NSSLS may be failed in the segmentation, since the NSSLS achieves segmentation results by minimizing the energy function just based on the similarity set scores of BUS image. In contrast, the proposed NSSRG employes two stop criterions: (1) $Score_{mean}(S) \geq 0.5Score_{mean}(I)$, where $Score_{mean}(S)$ and $Score_{mean}(I)$ represent the mean similarity set scores of the seed region and the whole image I, respectively; (2) $Intensity_{mean}(S) \geq 0.7Intensity_{mean}(H)$, where $Intensity_{mean}(S)$ and $Intensity_{mean}(H)$ represent the mean intensity value of the seed region and the whole image H, respectively. During the region growing procedure, the strict stop criterions can prevent the over-segmentation to the shadow regions and image border. Furthermore, a deep convolutional neural network used for false positive reduction also can avoid the over-segmentation on some extend. Thus,

This article has been accepted for publication in a future issue of this journal, but has not been fully edited. Content may change prior to final publication. Citation information: DOI 10.1109/ACCESS.2019.2911560, IEEE Access

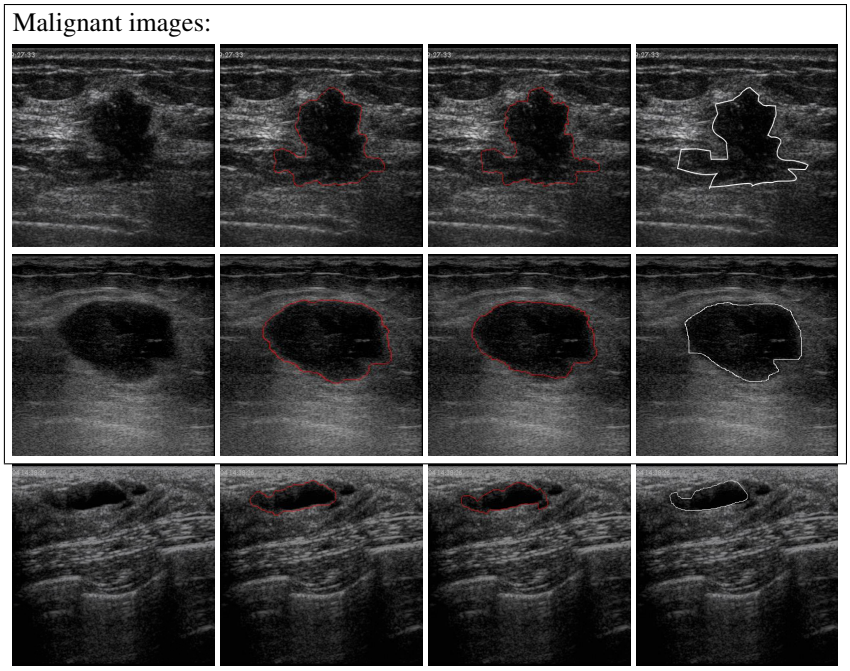

(a) (b) (c) (d)

FIGURE 4: Results of tumor segmentation with different methods: (a) original images; (b) Results of NSSRG method; (c) Results of NSSLS method; (d) Radiologist's results

the NSSRG can performe better than NSSLS for similar images, which are commonly in clinical practice.

Table 1 demonstrates the mean PDC, TPR, FPR, HD of the segmentation result on all the 86 testing images. It is observed that, compared to the NSSLS, the PDC and TPR of NSSRG were improved from 71.6±25.9%, 82.6±234.3% to 83.3±7.6%, 81.3±22.6%, and the FPR and HD of NSSRG were decreased from 95.8±234.3%, 113.0±98.0 $pixel$ to 13.5±22.6%, 54.7±41.6 $pixel$, respectively.

To show the comparison results between NSSLS and NSSRG intuitively, Fig. 6(a)-(d) illustrates the cumulative percentage of images having PDC, TPR, FPR and HD smaller/larger than a certain value on the segmentation results of NSSLS and NSSRG. As shown in Fig. 6, 80% images have PDC > 78%, HD < 90 $pixel$ and 90% images have TPR > 40%, FPR < 40% using NSSRG method.

To analyze the segmentation performances in the benign and malignant images, the mean and standard deviation of four quantitative metrics: PDC, TPR, FPR, HD are calculated on the benign and malignant images, individually, and collected in Table 2. It is observed that, 1) For NSSLS and NSSRG, the segmentation results achieve in benign images are better than that in malignant images; 2) The NSSRG always performs superior than NSSLS in benign images and malignant images.

Fig. 7 and Fig. 8 show the cumulative percentage of images with PDC, TPR, FPR and HD larger/smaller than a certain value on BUS images with benign and malignant tumors,

TABLE 1: The performances of computer segmentation results with reference to an experienced radiologist's manually drawn boundaries for the proposed method and the NSSLS method.

Methods	PDC (%)	TPR (%)	FPR (%)	Hausdorff Distance ($pixel$)
NSSRG	83.3 ± 7.6	81.3 ± 22.6	13.5 ± 22.6	54.7 ± 41.6
NSSLS	71.6 ± 25.9	82.6 ± 234.3	95.8 ± 234.3	113.0 ± 98.0

TABLE 2: The performances of computer segmentation results with reference to an experienced radiologist's manually drawn boundaries for the proposed method and the NSSLS method in the benign images and the malignant images.

	Methods	PDC (%)	TPR (%)	FPR (%)	Hausdorff Distance ($pixel$)
Benign images	NSSRG	81.6 ± 6.9	77.0 ± 20.3	11.2 ± 20.4	57.5 ± 46.1
	NSSLS	63.9 ± 30.1	73.4 ± 134.3	88.4 ± 134.0	146.9 ± 111.4
Malignant images	NSSRG	84.4 ± 7.8	84.3 ± 23.5	15.2 ± 23.5	52.8 ± 38.1
	NSSLS	77.2 ± 20.7	89.4 ± 283.1	101.1 ± 283.1	88.6 ± 78.6

This article has been accepted for publication in a future issue of this journal, but has not been fully edited. Content may change prior to final publication. Citation information: DOI 10.1109/ACCESS.2019.2911560, IEEE Access

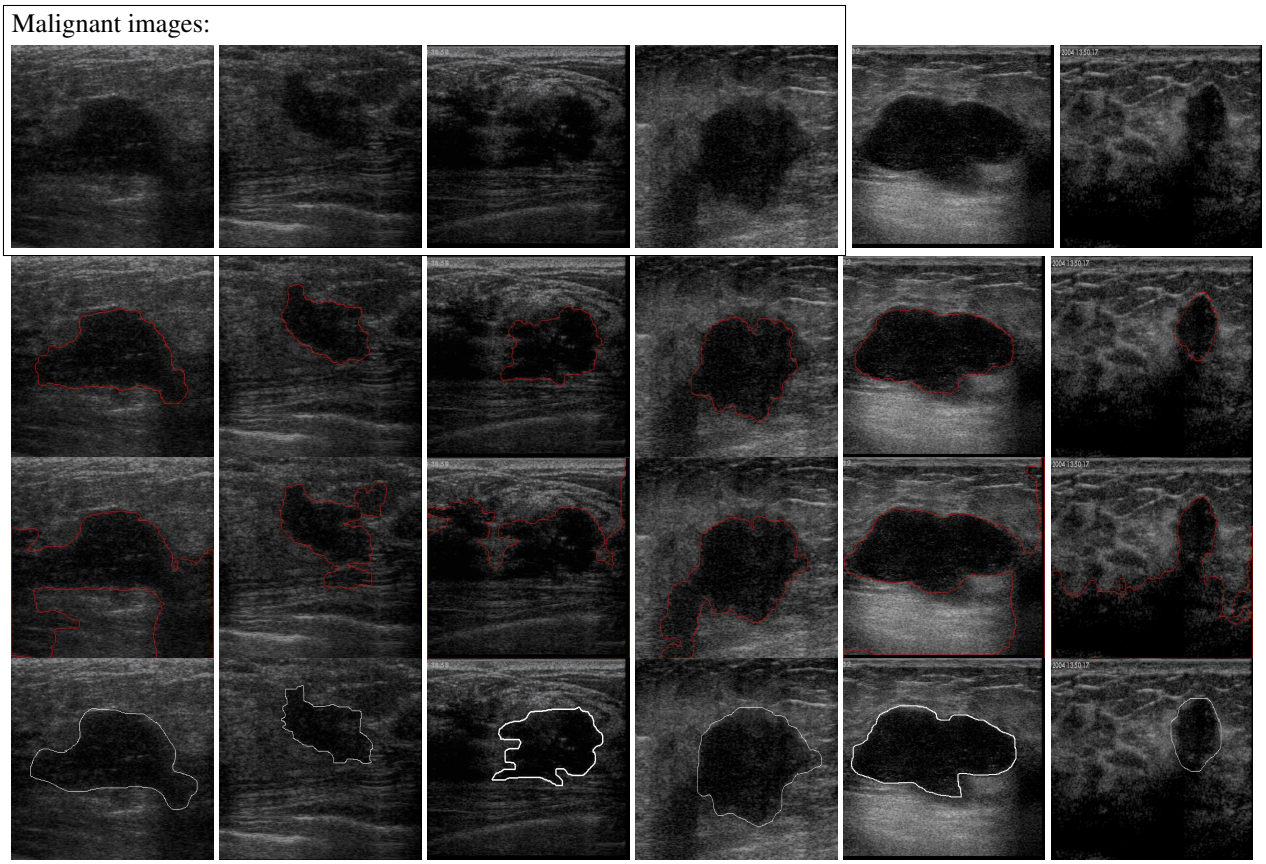

FIGURE 5: Results of tumor segmentation with different methods. Row1: original images; Row2: Results of NSSRG method; Row3: Results of NSSLS method; Row4: Radiologist's results

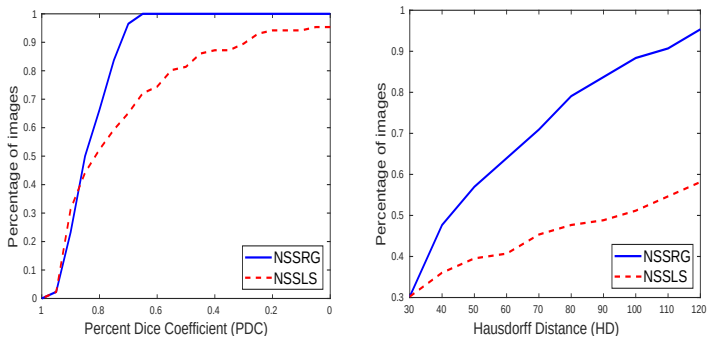

(a) percent dice coefficient (PDC) (b) Hausdorff distance (HD)

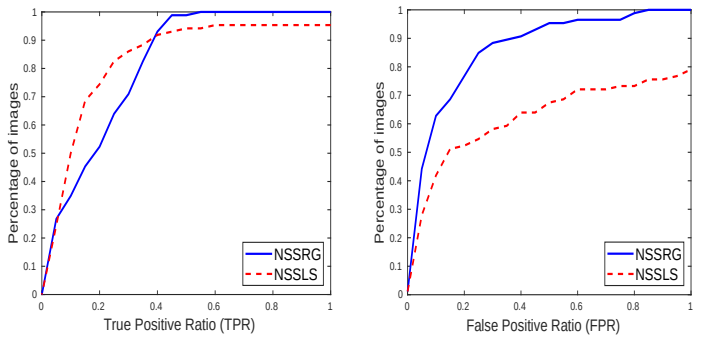

(c) true positive ratio (TPR) (d) false positive ratio (FPR)

FIGURE 6: Cumulative percentage relative to the 86 images with the radiologist's outlined tumor region as reference standards

This article has been accepted for publication in a future issue of this journal, but has not been fully edited. Content may change prior to final publication. Citation information: DOI 10.1109/ACCESS.2019.2911560, IEEE Access

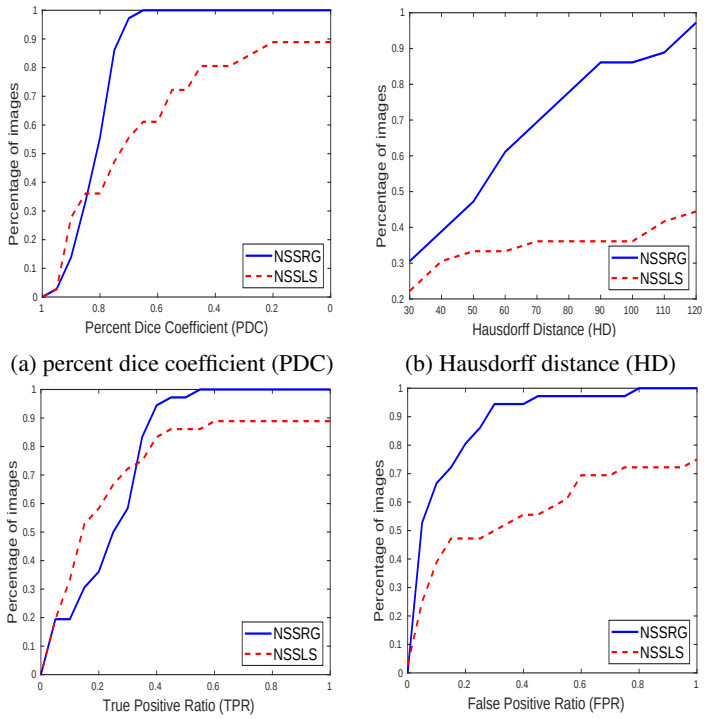

(a) percent dice coefficient (PDC) (b) Hausdorff distance (HD)

(c) true positive ratio (TPR) (d) false positive ratio (FPR)

FIGURE 7: Cumulative percentage relative to the 36 benign images with the radiologist's outlined tumor region as reference standards

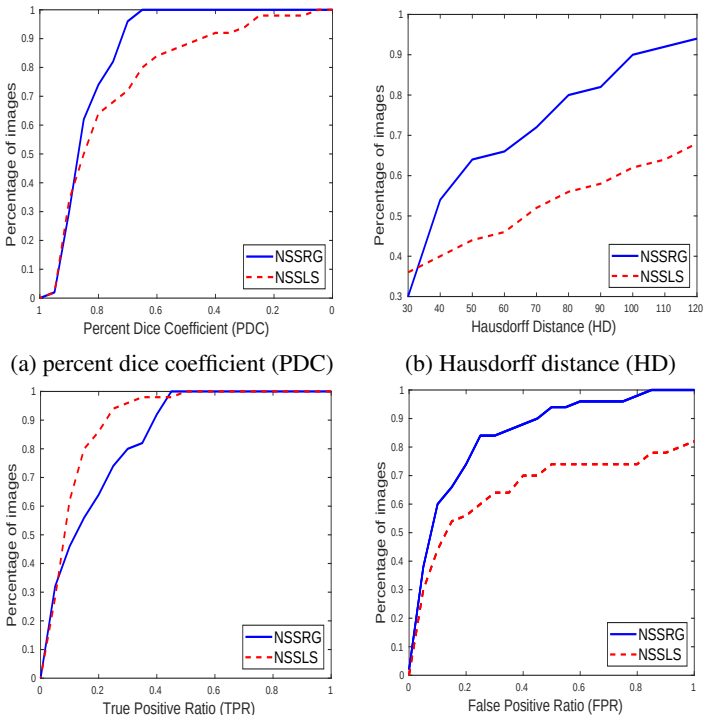

(a) percent dice coefficient (PDC) (b) Hausdorff distance (HD)

(c) true positive ratio (TPR) (d) false positive ratio (FPR)

FIGURE 8: Cumulative percentage relative to the 50 malignant images with the radiologist's outlined tumor region as reference standards

respectively. Among all the benign cases, in the results achieved by NSSRG, 80% images have PDC > 75%, HD < 90 $pixel$ and 90% images have TPR > 43%, FPR < 25%. In contrast, for the segmentation results achieved by NSSLS, 80% images have PDC > 37%, HD < 120 $pixel$ and 90% images have TPR > 40%, FPR < 80%. The Fig. 8 shows that 80% malignant images have PDC > 78%, HD < 80 $pixel$ and 90% images have TPR > 40%, FPR < 25% using NSSRG method. Furthermore, The NSSRG also performs better than NSSLS.

To analyze the segmentation results' performance in the images without tumor, additional thirty-five BUS images from thirty-five patients are collected from the fifth affiliated hospital of Sun Yat-Sen University for NSSRG segmentation test. There are three images with tumor segmented by NSSRG, which are regarded as misdiagnosed cases. Thus the false positive ratio on patient cases is 8.57%. Moreover, no tumor is missed among the segmentations on 86 test images with single tumor. Thus, the false negative ratio is much smaller than the false positive ratio but still needs to be evaluated on more cases.

The above experiment results and quantitative evaluations on various clinical BUS images demonstrate that the NSSRG method is effective and reliable in breast tumor segmentation, and also superior than NSSLS.

IV. CONCLUSION

An adaptive region growing method based on neutrosophic set (NSSRG) is proposed for brest ultrasound image segmentation in this study. By transforming the BUS images into NS domain, the similarity set score and homogeneity value for each pixel are calculated to characterize each pixel of BUS image. An adaptive Otsu-based thresholding method and morphology methods are used for generating the seed regions, then an adaptive region growing method is adapt based on the neutrosophic set for candidate tumor regions generation. A deep convolutional neural network, based on VGG-16 net, is used for false positive reduction and achieves the final segmentation result. Compared to the NSSLS method, the improved segmentation performances on 86 clinical BUS images illustrate that the NSSRG method is effective and robust for breast tumor segmentation on BUS images, especially for these tumors with blur and low contrast boundaries.

REFERENCES

[1] Huang, Q.L.Y.Z., Automatic Breast Ultrasound Image Segmentation: A Survey. Int J CARS, 2017. 12: p. 493-507.

[2] Drukker, K., et al., Computerized detection and classification of cancer on breast ultrasound. Academic Radiology, 2004. 11(5): p. 526-535.

[3] Cheng, H.D., et al., Automated breast cancer detection and classification using ultrasound images: A survey. Pattern Recognition, 2010. 43(1): p. 299-317.

[4] Drukker, K., N.C. Gruszauskas and M. Giger, Breast US computer-aided diagnosis workstation: performance with a large clinical diagnostic population. Radiology, 2008. 248(2): p. 392-397.

[5] K, H., et al., Computerized diagnosis of breast lesions on ultrasound. Medical Physics, 2002. 29(2): p. 157-164.

[6] Bo, L., et al., Automated segmentation of ultrasonic breast lesions using statistical texture classification and active contour based on probability distance. Ultrasound in Medicine & Biology, 2009. 35(8): p. 1309-1324.

[7] Fang, L., et al., Active contour model driven by global and local intensity information for ultrasound image segmentation. Computers & Mathematics with Applications, 2018. 75(12): p. 4286-4299.

[8] Guo fang, X., et al., Segmentation of ultrasound B-mode images with intensity inhomogeneity correction. IEEE Transactions on Medical Imaging, 2002. 21(1): p. 48-57.

[9] Chiao, L., et al., Computer-aided multiview tumor detection for automated whole breast ultrasound. Ultrasonic Imaging, 2014. 36(1): p. 3.

[10] Cortes, C. and V. Vapnik, Support-vector networks. Machine Learning, 1995. 20(3): p. 273-297.

[11] Liu, B., et al., Fully automatic and segmentation-robust classification of breast tumors based on local texture analysis of ultrasound images. Pattern Recognition, 2010. 43(1): p. 280-298.

[12] Othman, A.A. and H.R. Tizhoosh, Segmentation of Breast Ultrasound Images Using Neural Networks. 2011. 363(2): p. 260-269.

[13] Shan, J., Y. Wang and H.D. Cheng. Completely automatic segmentation for breast ultrasound using multiple-domain features. in IEEE International Conference on Image Processing. 2010.

[14] Yap, M.H., et al., Automated Breast Ultrasound Lesions Detection Using Convolutional Neural Networks. IEEE Journal of Biomedical and Health Informatics, 2018. 22(4): p. 1218-1226.

[15] Hiramatsu, Y., et al. Automated detection of masses on whole breast volume ultrasound scanner: false positive reduction using deep convolutional neural network. 2017: SPIE.

[16] Liu, Y., et al., Fully automatic Breast ultrasound image segmentation based on fuzzy cellular automata framework. Biomedical Signal Processing and Control, 2018. 40: p. 433-442.

[17] Guo, Y., A. Şengür and J. Tian, A novel breast ultrasound image segmentation algorithm based on neutrosophic similarity score and level set. Computer Methods and Programs in Biomedicine, 2016. 123: p. 43-53.

[18] Guo, et al., A Novel Color Image Segmentation Approach Based on Neutrosophic Set and;Modified Fuzzy c-Means. Circuits Systems & Signal Processing, 2013. 32(4): p. 1699-1723.

[19] Hojjatoleslami, S.A. and J. Kittler, Region growing: a new approach. IEEE Transactions on Image Processing A Publication of the IEEE Signal Processing Society, 1998. 7(7): p. 1079.

[20] Adams, R. and L. Bischof, Seeded Region Growing. IEEE Transactions on Pattern Analysis & Machine Intelligence, 2002. 16(6): p. 641-647.

[21] Fan, et al., Seeded region growing: an extensive and comparative study. Pattern Recognition Letters, 2017. 26(8): p. 1139-1156.

[22] Simonyan, K. and A. Zisserman, Very Deep Convolutional Networks for Large-Scale Image Recognition. Computer Science, 2014.

[23] Hinton G E , Srivastava N , Krizhevsky A , et al. Improving neural networks by preventing co-adaptation of feature detectors[J]. Computer Science, 2012, 3(4):págs. 212-223.

[24] V. Nair and G. E. Hinton, "Rectified Linear Units Improve Restricted Boltzmann Machines," in international conference on machine learning, 2010, pp. 807-814.

[25] A. Krizhevsky, I. Sutskever, and G. E. Hinton, "ImageNet Classification with Deep Convolutional Neural Networks," in neural information processing systems, 2012, pp. 1097-1105.

XUE JIANG is a student of the School of Data and Computer Science, Sun Yat-sen University, Guangzhou, China. Her research interests include Ultrasound Image Processing and Computer Aided Diagnosis.

This article has been accepted for publication in a future issue of this journal, but has not been fully edited. Content may change prior to final publication. Citation information: DOI 10.1109/ACCESS.2019.2911560, IEEE Access

YANHUI GUO received his B. S. degree in Automatic Control from Zhengzhou University, China, M.S. degree in Pattern Recognition and Intelligence System from Harbin Institute of Technology, China, and Ph.D. degree in the Department of Computer Science, Utah State University, USA. He was a research follow in the Department of Radiology at the University of Michigan and an assistant professor in St. Thomas University. Dr. Guo is currently an assistant professor in the Department of Computer Science at the University of Illinois at Springfield. Dr. Guo has published more than 80 journal papers and 30 conference papers, completed more than 10 grant funded research projects, and worked as an associate editor of different international journals, reviewers for top journals and conferences. His research area includes computer vision, machine learning, big data analytics, computer aided detection/diagnosis, and computer assist surgery.

HAIBIN CHEN is a post-doctor in School of Data and Computer Science at San Yat-sen University. His interests range in medical image processing, radiotherapy technology and machine learning. During his Ph.D study period, he was invited as visiting researcher to the Department of Radiotherapy and Oncology at University of Texas SouthWestern Medical Center. His Ph.D researches focused on the applications of artificial intelligence in radiotherapy.

YAQIN ZHANG is an attending doctor in Radiology Department, the Fifth Affiliated Hospital, Sun Yat-sen University, Zhuhai, China. She received her M.D. degree from Sun Yat-sen University, China in 2008. Her research interests include abdominal and uro-radiology.

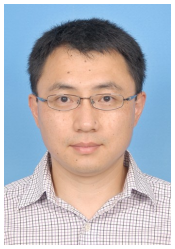

YAO LU is a Professor of the School of Data and Computer Science, Sun Yat-sen University, Guangzhou, China. He was a Postdoctoral Research Fellow and Research Investigator in Medical School, University of Michigan. His research interests include Inverse Problem, Medical Image Processing and Computer Aided Diagnosis.